CONDENSED MATTER PHYSICS

Cavity quantum-electrodynamical polaritonically enhanced electron-phonon coupling and its influence on superconductivity

M. A. Sentef[1]*, M. Ruggenthaler[1], A. Rubio[1,2]

So far, laser control of solids has been mainly discussed in the context of strong classical nonlinear light-matter coupling in a pump-probe framework. Here, we propose a quantum-electrodynamical setting to address the coupling of a low-dimensional quantum material to quantized electromagnetic fields in quantum cavities. Using a prototypical model system describing FeSe/$SrTiO_3$ with electron-phonon long-range forward scattering, we study how the formation of phonon polaritons at the two-dimensional interface of the material modifies effective couplings and superconducting properties in a Migdal-Eliashberg simulation. We find that through highly polarizable dipolar phonons, large cavity-enhanced electron-phonon couplings are possible, but superconductivity is not enhanced for the forward-scattering pairing mechanism due to the interplay between coupling enhancement and mode softening. Our results demonstrate that quantum cavities enable the engineering of fundamental couplings in solids, paving the way for unprecedented control of material properties.

INTRODUCTION

Strong coupling and manipulation of matter with photons in quantum-electrodynamical (QED) environments are becoming a major research focus across many disciplines. Among the topics with large potential are the creation of exciton-polariton condensates (*1*), polaritonic chemistry (*2*–*5*) and transport (*6*), quantum nanoplasmonics (*7*), light-induced topology (*8*–*10*) and magnetism in 2D materials (*11*), and novel spectroscopies (*12*). In condensed matter, the search for control knobs to design properties of quantum materials is an ongoing broad research effort (*13*). One possible route is to use the nonequilibrium dynamics and coherent manipulation of quantum many-body systems with ultrashort laser pulses (*14*–*23*). However, in these cases, "classical" light was typically used. Here, we propose a new route toward manipulating microscopic couplings in solids and inducing ordered phases especially at interfaces and in two-dimensional (2D) materials.

The discovery of enhanced superconductivity in monolayer FeSe on $SrTiO_3$ (*24*–*26*) and its possible relation to a cross-interfacial electron-phonon coupling (*27*–*29*) has stimulated considerable interest with an ongoing open debate (*30*–*35*). Irrespective of the outcome of this debate, the interfacial phonon mode under consideration is of particular interest for light-control purposes as it has a dipole moment implying bilinear phonon-photon coupling, while at the same time, the phonon also couples bilinearly to in-plane FeSe electrons, with a vertex that is strongly peaked for small momentum transfers known as forward scattering. This combination of features is due to the high degree of anisotropy owing to the interfacial structure. Here, we use a prototypical model system, related to FeSe/$SrTiO_3$, for this extreme forward scattering to investigate how photon-phonon coupling in cavities can affect electron-phonon coupling and phonon-mediated superconductivity.

[1]Max Planck Institute for the Structure and Dynamics of Matter, Center for Free Electron Laser Science, 22761 Hamburg, Germany. [2]Center for Computational Quantum Physics (CCQ), The Flatiron Institute, 162 Fifth Avenue, New York, NY 10010, USA.
*Corresponding author. Email: michael.sentef@mpsd.mpg.de

RESULTS

Setup: 2D material inside a cavity

In Fig. 1A, we show the setup for a 2D material inside a QED cavity environment with perfectly reflecting mirrors. The mirrors confine the photon modes inside the cavity and can lead to strong light-matter coupling even when only the vacuum of the electromagnetic field is considered (*36*, *37*). Specifically, we propose a layered structure of a 2D material (e.g., monolayer FeSe) on a dielectric substrate with a large dielectric constant (e.g., $SrTiO_3$) that further helps confine the cavity photon modes of interest.

For the particular example of FeSe/$SrTiO_3$, the effect of the cavity is to couple the electromagnetic field of the photons polarized along the z direction, perpendicular to the interfacial plane, to a cross-interfacial phonon mode. Here, we go beyond the often-used rotating-wave and dipole approximations for the light-matter interaction and use full minimal dipolar coupling including the $J \cdot A$ and A^2 terms (see section S2), which makes the theory manifestly gauge invariant and avoids unphysical divergences. The phonon has a dipole moment along the z direction that involves motion of the O and Ti ions in the topmost layer of $SrTiO_3$, spatially very close to the FeSe monolayer. Specifically, one quasi-dispersionless optical Fuchs-Kliewer phonon at 92 meV (*29*) was identified as the most relevant phonon mode that strongly couples to the FeSe electrons both in angle-resolved photoemission (*27*) and high-resolution electron energy loss spectroscopies (*29*). The influence of screening on this mode is not settled yet, particularly when it comes to phonon linewidths (*30*, *31*). However, the experimental evidence for its influence on electronic properties (*27*, *29*) is definitely present, suggesting use of this mode to build a simplified model Hamiltonian to address the impact of reaching strong light-matter coupling on the superconducting behavior of the material. We specifically use a single-band model for the electrons in two spatial dimensions in a partially filled band with filling $n = 0.07$ per spin, as previously used to model the relevant electronic structure fitting angle-resolved photoemission data (*28*). A bilinear electron-phonon scattering is introduced by a coupling vertex $g(\vec{q}) = g_0 \exp(-|\vec{q}|/q_0)$ that is strongly peaked near momentum $\vec{q} = 0$ with a coupling range q_0. The coupling strength g_0 is adjusted to keep a total dimensionless coupling strength $\lambda \approx 0.18$ independent of q_0, where λ is determined from the effective electronic mass renormalization

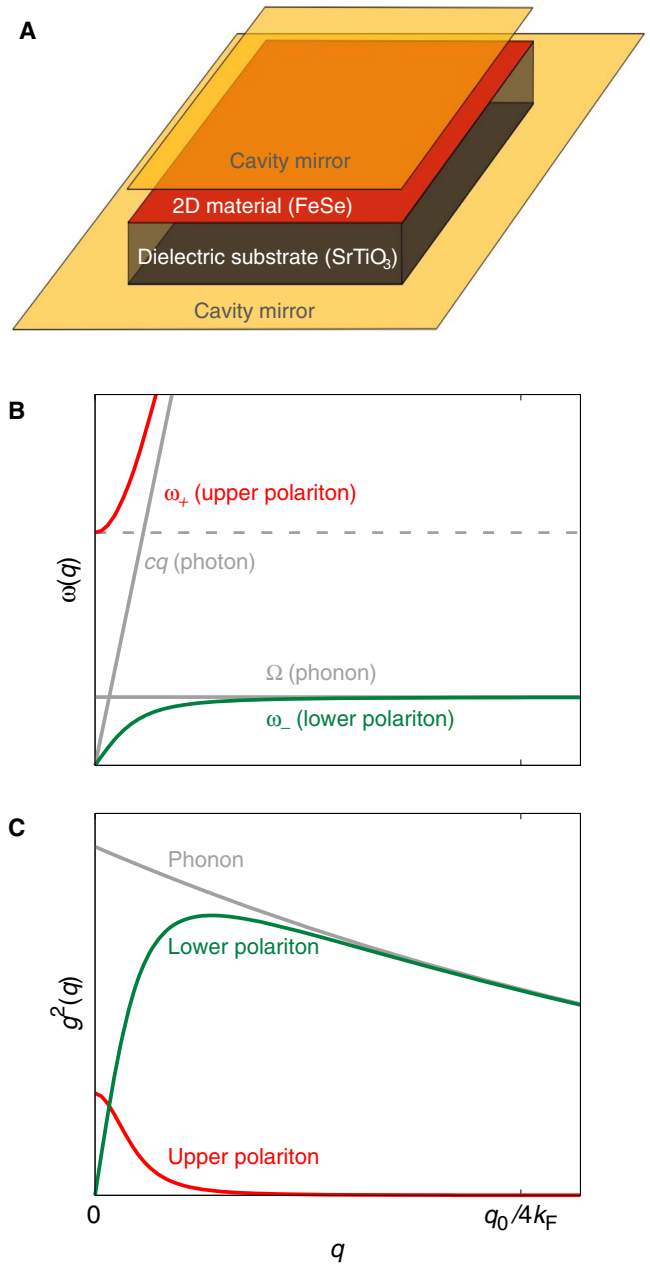

Fig. 1. Setup of 2D material in optical cavity, phonon polariton frequency dispersions, and momentum-dependent electron-phonon coupling vertices for the polariton branches. (**A**) We consider a setup with a 2D material on a dielectric substrate inside a small optical cavity with mirrors as shown. (**B**) Schematic phonon, photon, and upper and lower polariton dispersions versus 2D in-plane momentum q. The coupling of the phononic dipole current to the photonic vector potential leads to a splitting determined by the plasma frequency ω_P. In the cavity, ω_P is controlled by the cavity volume. (**C**) Momentum-dependent squared electron-boson vertex $g^2(q)$. For forward scattering, the squared bare electron-phonon vertex $g^2(q) = g_0^2\exp(-2q/q_0)$ is peaked near $q = 0$. In the polaritonic case ($\omega_P > 0$), the upper polariton branch inherits some of the electron-phonon coupling at small q.

$m^*/m = 1 + \lambda$ in the metallic normal state above the superconducting critical temperature in the absence of the cavity coupling. This conservative choice of λ is, for instance, below the value of 0.25 that was given in (*29*).

Through phonon-photon coupling, we study phonon-polariton formation in this setting. In Fig. 1B, we show schematically the resulting polariton branches that stem from a gauge-invariant coupling involving both $J \cdot A$ and A^2 terms, where J is the current of phononic dipoles associated to an infrared-active phonon mode, and A is the electromagnetic gauge field of the photons. The relevant effective coupling strength between photons and phonons is given by the phononic plasma frequency $\omega_P = \sqrt{\frac{4\pi e^2}{M v_{0,2D} L_z}}$, with M as the reduced mass of the phonon (see section S2). For the 2D system in the cavity, the plasma frequency is controlled by the length of the vacuum inside the cavity in the z direction, L_z, and the 2D unit cell area $v_{0,2D} = L_x L_y / N_x N_y$, with L_i and N_i as the length and number of unit cells of the system in i direction, respectively. The plasma frequency sets the splitting between the upper and lower polariton branches, reminiscent of the LO-TO splitting in bulk semiconductors. Obviously, this splitting is only relevant at very small momenta q, since the photon energies quickly become large compared to the phonon frequency as q increases because of the large magnitude of the speed of light.

The formation of phonon polaritons leads to a redistribution of the electron-phonon coupling vertex into the two polariton branches. In the following, we refer to this coupling between electrons and phonon polaritons as "electron-phonon coupling," since the coupling originates from electron-phonon coupling in the free-space setting without cavity, and direct electron-photon coupling is not relevant in our setup. In Fig. 1C, we plot the squares of the coupling vertices between electrons and the respective polaritons as a function of q/k_F, where k_F is the Fermi momentum. A realistic value of the coupling range for FeSe/$SrTiO_3$ was estimated as $q_0/k_F \approx 0.1$, as needed to create replica bands in angle-resolved photoemission that duplicate primary band features without substantial momentum smearing (*27*, *28*). In a microscopic model, this value depends on the distance h_0 between the topmost TiO_2 layer and the FeSe monolayer as well as the anisotropy of in-plane and perpendicular dielectric constants via $q_0^{-1} = h_0\sqrt{\epsilon_\parallel/\epsilon_\perp}$, with realistic estimates $\epsilon_\parallel/\epsilon_\perp \approx 100$ and $1/(h_0 k_F) \approx 1$. This coupling range is larger than the momentum at which photon and phonon branches cross and mix most strongly in the polariton formation process. This implies that the modification of electron-phonon coupling due to the cavity only happens at very small momenta typically smaller than q_0/k_F. Thus, to investigate how the degree of forward scattering influences the way in which cavity coupling is able to modify the electronic properties, we use different values for q_0/k_F below, envisioning that cavity effects are enhanced when q_0/k_F becomes smaller, which would, in practice, be achieved by making the dielectric-constant anisotropy ratio larger. In Table 1, we summarize the relevant parameter values of the bare material used in our simulations.

Cavity-enhanced electron-phonon interaction

The critical question to answer here is how the redistribution of the coupling vertex to the upper and lower polariton branches affects the electronic properties. We investigate this by a diagrammatic approach using Matsubara Green's functions. We adopt the same approximations used in (*28*) and compute the self-consistent Migdal-Eliashberg diagram with dressed electronic Green's function in Nambu space, allowing us to take into account superconducting order. The central quantity is the electronic self-energy $\hat{\Sigma}(\vec{k}, i\omega_n) = i\omega_n[1 - Z(\vec{k}, i\omega_n)]\hat{\tau}_0 + \chi(\vec{k}, i\omega_n)\hat{\tau}_3 + \phi(\vec{k}, i\omega_n)\hat{\tau}_1$, written in terms of the Pauli matrices $\hat{\tau}_i$, the effective mass renormalization $Z(\vec{k}, i\omega_n)$, the band dispersion renormalization

Table 1. Parameters of the bare material system without the cavity used for the simulations discussed in the main text.

Parameter set	A	B	C
Phonon frequency Ω (eV)	0.092	0.092	0.092
Electron-phonon coupling g_0 (eV)	2.25	4.455	11.1
Coupling range q_0/k_F	0.105	0.053	0.026
Dimensionless coupling strength λ at 116.5 K	0.180	0.180	0.180

$\chi(\vec{k}, i\omega_n)$, and the anomalous self-energy $\phi(\vec{k}, i\omega_n)$, which vanishes in the normal state.

We first investigate the effect of the cavity on the effective electron-phonon coupling λ itself. This is of interest independent of superconductivity to be discussed below, as the electron-phonon coupling affects many other properties of materials, such as the conductivity, structural phase transitions, or superconductivity in standard Bardeen-Cooper-Schrieffer (BCS) superconductors. In particular, it plays a pivotal role for terahertz-driven nonequilibrium phases of materials. In Fig. 2, we show how cavity coupling modifies the temperature-dependent quasiparticle mass renormalization obtained from the normal self-energy for the different coupling ranges, realistic $q_0/k_F = 0.105$ (Fig. 2A), reduced $q_0/k_F = 0.053$ (Fig. 2B), and very small $q_0/k_F = 0.021$ (Fig. 2C). The first observation is that independent of the cavity, λ shows a strong temperature dependence, with a peak around T_c, decreasing both toward higher temperatures and toward lower temperatures deep inside the ordered phase. The former is readily understood as a usual temperature effect when at high temperature, the system becomes more and more classical and less correlated. The latter is understood by considering the fact that correlation effects are reduced deep in the ordered phase when quantum fluctuations lose their importance and a quasi-classical mean-field description can be adopted. λ is enhanced by the cavity at all temperatures. The cavity effects are more pronounced as ω_P increases for fixed q_0/k_F and as q_0/k_F decreases for fixed ω_P.

Light-modified superconductivity

We now turn to the effect of the cavity on superconductivity. Naively, one might expect that an enhanced λ leads to enhanced superconducting critical temperature T_c. However, the relation is nontrivial as also the effective polariton frequency is relevant for T_c. We will see in the following that, unfortunately, for our system, the enhancement of λ is canceled by a reduction in the effective frequency.

Figure 3A shows the resulting temperature-dependent superconducting order gap $\Delta \equiv \phi(\vec{k}_F, i\pi/\beta)/Z(\vec{k}_F, i\pi/\beta)$ evaluated at the smallest Matsubara frequency and at a Fermi momentum $\vec{k}_F \approx (0.666/a, 0.666/a)$ along the Brillouin zone diagonal for a coupling range $q_0/k_F = 0.105$ representative of $FeSe/SrTiO_3$. Starting from a critical temperature $T_c \approx 63$ K in the absence of the cavity ($\omega_P = 0.0$), we find a slight reduction of superconductivity as the cavity is introduced and its extension L_z in the z direction perpendicular to the 2D material is reduced, resulting in a nonzero $\omega_P \propto 1/\sqrt{L_z}$. For perhaps unrealistically large values $\omega_P = 5.0$ (eV), a reduction of T_c on the order of 1 K is found in our simulations, which would likely require cavity sizes of a few lattice constants and might, in practice, be too small to achieve at the moment.

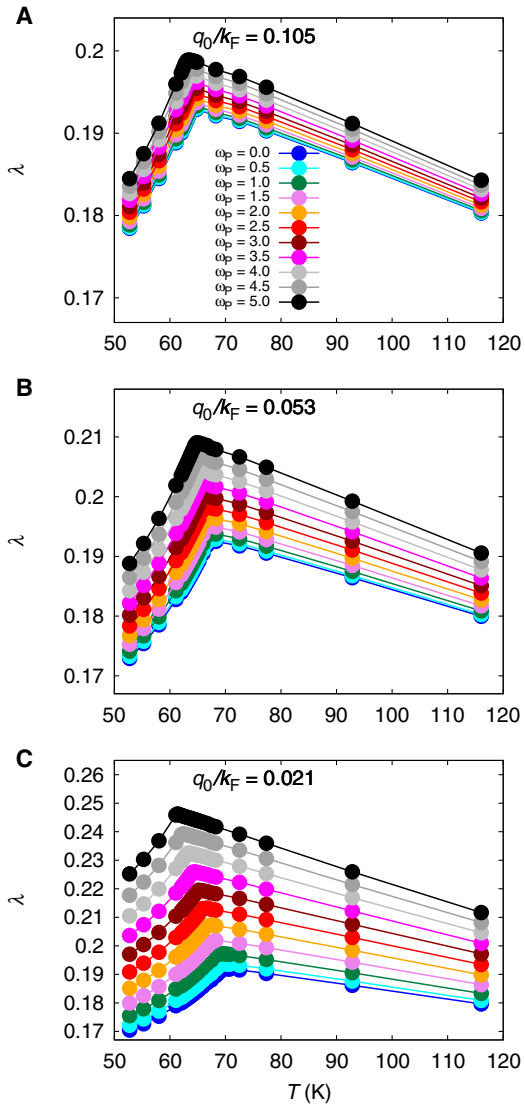

Fig. 2. Temperature-dependent electron-phonon coupling for different coupling ranges and plasma frequencies. (**A**) Dimensionless electron-phonon coupling strength extracted from the normal self-energy at $\vec{k}_F$ at the smallest Matsubara frequency, $\lambda \equiv Z(\vec{k}_F, i\pi/\beta) - 1$, as a function of temperature for a value of the coupling range in momentum space $q_0/k_F = 0.105$ representative of $FeSe/SrTiO_3$, and different phononic plasma frequencies ω_P as indicated. The case $\omega_P = 0$ represents the system without cavity. For increasing ω_P, λ increases. Below the superconducting transition, which also shifts with ω_P (see Fig. 3), λ decreases consistently for all values of ω_P. (**B**) Temperature-dependent λ for smaller $q_0/k_F = 0.053$ and different ω_P. As for the superconducting order parameter, the effects of the cavity coupling that is parameterized by ω_P are more pronounced. (**C**) For even smaller $q_0/k_F = 0.021$, we obtain a strongly enhanced λ accompanied by the shift in the superconducting transition that shows up as a cusp in $\lambda(T)$, which reaches a maximum at T_c.

To investigate the effect of the forward-scattering coupling range, we look at the change of the superconducting order in the case of $q_0/k_F = 0.053$ that is reduced by a factor of 2 from the realistic value described above (see Fig. 3B). In this case, the polaritonic redistribution of the coupling is expected to be more effective, as there is a better match between the coupling range and the polariton mixing. This is observed in the superconducting order enhancement. Where a value of $\omega_P = 5.0$ was

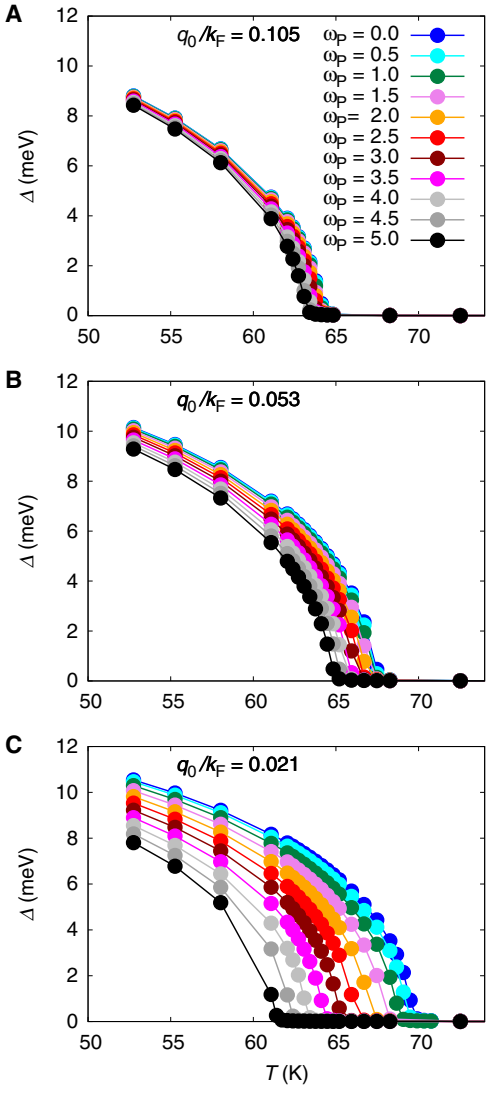

Fig. 3. Temperature-dependent superconducting gap for different coupling ranges and plasma frequencies. (**A**) The superconducting gap at $\vec{k}_F$ at the smallest Matsubara frequency, $\Delta \equiv \phi(\vec{k}_F, i\pi/\beta)/Z(\vec{k}_F, i\pi/\beta)$, as a function of temperature for a value of the coupling range in momentum space q_0/k_F = 0.105 representative of FeSe/$SrTiO_3$, and different phononic plasma frequencies ω_P (measured in electron volts for the FeSe example) as indicated. The case ω_P = 0 represents the system without cavity. For the decreasing cavity volume, ω_P increases, causing a decrease in Δ and the superconducting critical temperature T_c. (**B**) Temperature-dependent gap for smaller q_0/k_F = 0.053 and different ω_P. The light-suppressed superconductivity is more pronounced. (**C**) For even smaller q_0/k_F = 0.021, strongly reduced Δ values are observed with increasing ω_P.

needed in Fig. 3A to obtain a visible modification of T_c, here, a smaller value ω_P = 2.5 is sufficient to enhance T_c by ≈1 K. Even larger ω_P leads to enhancements of order 5%. Last, if we decrease the range by another factor of 2, q_0/k_F = 0.021, the modification is relatively strong with changes of more than 10%, shifting T_c by up to 10 K (Fig. 3C).

Analysis of the influence of the cavity on superconductivity

To gain physical intuition into why the enhancement of λ is insufficient to enhance superconductivity, we take a look at the approximate equation for T_c derived by Rademaker *et al.* (*28*) in the extreme forward-scattering and weak-coupling limit

$$T_C \approx \frac{\lambda\Omega}{2+3\lambda} \quad (1)$$

From this expression, it becomes clear that the enhancement of λ has to be sufficiently strong compared to the suppression of Ω that happens concomitantly in our case. This should be contrasted with the standard expression for a momentum-independent coupling vertex in the BCS theory, $T_{c,BCS} \approx 1.13\Omega\exp(-\frac{1}{\lambda})$. The quasi-linearity in λ in Eq. 1 leads to relatively high T_c for moderate values of λ but, in the cavity, also has the negative effect that the enhancement of T_c scales only linearly rather than exponentially with λ.

DISCUSSION

Unfortunately, the enhancement of λ predicted here does not lead to an enhancement of the superconducting critical temperature T_c in our chosen setting. This effect is explained by the linear scaling of the critical temperature with λ for the case of extreme forward scattering in contrast to the exponential scaling for momentum-independent coupling. However, for more conventional pairing mechanisms not geared toward forward scattering, the observed enhancement of λ could naturally lead to enhanced T_c. Similarly, in dirty superconductors, momentum-conservation constraints are relaxed, which may lead to enhancement rather than suppression of T_c, as discussed in a slightly different context in (*38*).

Moreover, our theory and the analytical estimates of T_c are valid only in the Migdal-Eliashberg regime of weak coupling, unrenormalized polaritons, and adiabaticity. A polaritonic enhancement of λ could still lead to the enhancement of T_c even for the forward-scattering case at intermediate couplings, when feedback effects on the polaritons become important and when nonadiabatic effects come into play. Similarly, interplay between polaritonic pairing and other pairing mechanisms such as spin or orbital fluctuations is a subject for future study. It is possible that in these cases, our original motivation of this work, namely to enhance superconductivity in a cavity, might work out.

In summary, we propose to use QED cavity settings to control polaritonically mediated effects in low-dimensional materials. In reality, the size of the achieved effects will depend on the quality factor of the cavity, the degree to which our idealized boundary conditions are realized in practice, and on the required large coupling strengths that can actually be reached in real devices. However, our above results are ground-state modifications that are still qualitatively valid even in dissipative systems (*5*, *39*). Moreover, for organic molecules in cavities, the ultrastrong-coupling regime was even achieved in bad cavities with small quality factors (*40*). Here, we predict changes of T_c in a few percent range for few-percent changes of the electron-phonon coupling λ. Known examples of LO-TO splitting in bulk semiconductors such as GaP suggest typical ratios of ω_P/Ω of order 10% (*41*), an order of magnitude smaller than the ones used in this work. However, we caution that these are very different materials from the ones used here, and oxide dielectrics close to the ferroelectric phase transition, such as $SrTiO_3$, were suggested to have giant LO-TO splittings exceeding 50% of the TO frequency (*42*) due to enhanced Born effective charges, placing them much closer to the values explored here. It remains to be answered how large realistic LO-TO splittings can

become at interfaces. It will definitely be important to explore strategies for enhancing the plasma frequency by synthesizing samples using different substrates with strongly coupled polar phonons and exploring interface and heterostructure engineering to optimize the dielectric environment.

We note that a related idea of exciton-mediated superconducting pairing (*43*) in 2D heterostructures was introduced (*44*) and recently discussed in the context of transition-metal dichalcogenides (*45*). These proposals require exciton-polariton condensates to exist in the first place, which then affect pairing in doped nearby layers via coupling of quasi-free electrons to condensed exciton polaritons. By contrast, our present proposal does not rely on bosonic condensation but rather focuses on directly modifying the electron-phonon coupling through polariton formation in a cavity. For the example of FeSe/$SrTiO_3$, our proposal could help shed light on the abovementioned debate about the role of the forward-scattering phonon for superconductivity. If the coupling of the phonon to electrons is unimportant, then the polaritonic effects will not play a role, which could serve as a test for the influence of the phonon on the electronic properties. Similarly, it was recently suggested to use classical lasers in a pump-probe setting to study the forward-scattering nature of the phonon (*46*). Ongoing work focuses on a realistic ab initio computation of cavity-enhanced couplings via dipolar phonons using the framework of QED density functional theory (*47*).

Note added in revision

Upon revision of the manuscript, we became aware of two related works that discuss related ideas of modifying superconducting properties by electron-photon interactions in cavities (*38*, *48*).

MATERIALS AND METHODS

We used a cavity QED setting with plane-wave mode expansion inside a cavity, with fixed-node boundary conditions for confined cavity photon modes along the z direction and periodic boundary conditions in the extended 2D plane (see section S1). Specifically, we use the Migdal-Eliashberg approximation to the electronic self-energy to a coupled electron-polariton model Hamiltonian involving electron-phonon forward scattering and dipolar phonon-photon coupling.

The electron-polariton Hamiltonian has the form

$$H = \sum_{\vec{k},\sigma} \epsilon_{\vec{k}} c^{\dagger}_{\vec{k},\sigma} c_{\vec{k},\sigma} + \frac{1}{\sqrt{N}} \sum_{\vec{k},\vec{q},\sigma,\lambda=\pm} c^{\dagger}_{\vec{k}+\vec{q},\sigma} c_{\vec{k},\sigma} \left(g^{*}_{\lambda}(\vec{q}) \alpha^{\dagger}_{-\vec{q},\lambda} + g_{\lambda}(\vec{q}) \alpha_{\vec{q},\lambda} \right) + \sum_{\vec{q},\lambda=\pm} \omega_{\lambda}(\vec{q}) \alpha^{\dagger}_{\vec{q},\lambda} \alpha_{\vec{q},\lambda}$$

with $c^{\dagger}_{\vec{k},\sigma}$ ($c_{\vec{k},\sigma}$) as the electron creation (annihilation) operators at wave vector $\vec{k}$ and spin σ and $\epsilon_{\vec{k}} = -2t[\cos(k_x a) + \cos(k_y a)] - \mu$ as the electronic band dispersion measured relative to the chemical potential μ, which was adjusted to fix a band filling of 0.07 per spin. Furthermore, N is the number of k points in the 2D Brillouin zone, and $g_{\lambda}(\vec{q})$ is the polariton-momentum $\vec{q}$-dependent electron-polariton coupling to branch λ = ±

$$g_{+}(\vec{q}) = i\sin(\theta_{\vec{q}}) \sqrt{\frac{\omega_{+}(\vec{q})}{\Omega}} g_0 \exp(-|\vec{q}|/q_0) \tag{2}$$

$$g_{-}(\vec{q}) = i\cos(\theta_{\vec{q}}) \sqrt{\frac{\omega_{-}(\vec{q})}{\Omega}} g_0 \exp(-|\vec{q}|/q_0) \tag{3}$$

with bosonic polariton creation (annihilation) operators $\alpha_{\vec{q},\lambda}$ ($\alpha^{\dagger}_{\vec{q},\lambda}$) for the polaritons with energies

$$\omega_{\pm}(\vec{q}) = \left(\frac{1}{2} \left(\omega_{\mathrm{phot}}(\vec{q})^2 + \omega_{\mathrm{p}}^2 + \Omega^2 \pm \sqrt{(\omega_{\mathrm{phot}}(\vec{q})^2 + \omega_{\mathrm{p}}^2 + \Omega^2)^2 - 4\omega_{\mathrm{phot}}(\vec{q})^2 \Omega^2} \right) \right)^{\frac{1}{2}} \tag{4}$$

The unitary transformation from phonons and photons to polaritons is parameterized by

$$\arctan(\theta_{\vec{q}}) = \frac{\omega_{\mathrm{phot}}(\vec{q})^2 + \omega_{\mathrm{p}}^2 - \Omega^2 + \sqrt{(\omega_{\mathrm{phot}}(\vec{q})^2 + \omega_{\mathrm{p}}^2 + \Omega^2)^2 - 4\omega_{\mathrm{phot}}(\vec{q})^2 \Omega^2}}{2\Omega\omega_{\mathrm{p}}} \tag{5}$$

Here, the underlying bare energies are given by the electronic hopping t = 0.075 eV (*28*) and the phonon frequency Ω = 92 meV (*29*), and the bare photon dispersion is $\omega_{\mathrm{phot}}(\vec{q}) = c|\vec{q}|$ with speed of light c, and we used a variable effective phononic plasma frequency ω_{p} throughout the main text. Further details can be found in sections S2 and S3.

The Migdal-Eliashberg electronic self-energy on the Matsubara frequency axis is given by

$$\hat{\Sigma}(\vec{k}, i\omega_n) = \frac{-1}{N\beta} \sum_{\vec{q},m,\lambda=\pm} |g_{\lambda}(\vec{q})|^2 D^{(0)}_{\lambda}(\vec{q}, i\omega_n - i\omega_m) \hat{\tau}_3 \hat{G}(\vec{k}+\vec{q}, i\omega_m) \hat{\tau}_3,$$

with self-consistent electronic Nambu Green's function $\hat{G}$, decomposed into Pauli matrices $\hat{\tau}_i$, unrenomalized polaritonic Green's function $D^{(0)}$, and fermionic Matsubara frequencies $\omega_n = (2n+1)\pi/\beta$ and bosonic Matsubara frequencies $\omega_n = 2n\pi/\beta$, $n \in \mathbb{Z}$, and inverse temperature $\beta = (k_B T)^{-1}$. This amounts to the approximation that the bare phonon mode already contains the energy-shift renormalization due to electron-phonon coupling as the bare phonon frequency is taken from experimental data, and further renormalizations of the phonon polaritons due to electron-polariton coupling are small. The self-consistent computation of $\hat{\Sigma}$ was initialized with a seed for the anomalous superconducting self-energy of 0.007 eV and a convergence criterion of 10^{-6} eV. Further details can be found in section S4.

SUPPLEMENTARY MATERIALS

Supplementary material for this article is available at http://advances.sciencemag.org/cgi/content/full/4/11/eaau6969/DC1

Section S1. Relevant photon modes in cavity
Section S2. Phonon-photon Hamiltonian
Section S3. Electron-polariton Hamiltonian
Section S4. Migdal-Eliashberg simulations

REFERENCES AND NOTES

1. T. Byrnes, N. Y. Kim, Y. Yamamoto, Exciton-polariton condensates. *Nat. Phys.* **10**, 803–813 (2014).
2. J. Galego, F. J. Garcia-Vidal, J. Feist, Cavity-induced modifications of molecular structure in the strong-coupling regime. *Phys. Rev. X* **5**, 041022 (2015).
3. T. W. Ebbesen, Hybrid light-matter states in a molecular and material science perspective. *Acc. Chem. Res.* **49**, 2403–2412 (2016).
4. J. Flick, M. Ruggenthaler, H. Appel, A. Rubio, Kohn-Sham approach to quantum electrodynamical density-functional theory: Exact time-dependent effective potentials in real space. *Proc. Natl. Acad. Sci. U.S.A.* **112**, 15285–15290 (2015).
5. J. Flick, M. Ruggenthaler, H. Appel, A. Rubio, Atoms and molecules in cavities, from weak to strong coupling in quantum-electrodynamics (QED) chemistry. *Proc. Natl. Acad. Sci. U.S.A.* **114**, 3026–3034 (2017).
6. D. Hagenmüller, S. Schütz, J. Schachenmayer, C. Genes, G. Pupillo, Cavity-assisted mesoscopic transport of fermions: Coherent and dissipative dynamics. *Phys. Rev. B* **97**, 205303 (2018).
7. M. S. Tame, K. R. McEnery, Ş. K. Özdemir, J. Lee, S. A. Maier, M. S. Kim, Quantum plasmonics. *Nat. Phys.* **9**, 329–340 (2013).
8. N. H. Lindner, G. Refael, V. Galitski, Floquet topological insulator in semiconductor quantum wells. *Nat. Phys.* **7**, 490–495 (2011).
9. M. Claassen, C. Jia, B. Moritz, T. P. Devereaux, All-optical materials design of chiral edge modes in transition-metal dichalcogenides. *Nat. Commun.* **7**, 13074 (2016).
10. H. Hübener, M. A. Sentef, U. De Giovannini, A. F. Kemper, A. Rubio, Creating stable Floquet-Weyl semimetals by laser-driving of 3d Dirac materials. *Nat. Commun.* **8**, 13940 (2017).
11. D. Shin, H. Hübener, U. De Giovannini, H. Jin, A. Rubio, N. Park, Phonon-driven spin-Floquet magneto-valleytronics in MoS_2. *Nat. Commun.* **9**, 638 (2018).
12. M. Ruggenthaler, N. Tancogne-Dejean, J. Flick, H. Appel, A. Rubio, From a quantum-electrodynamical light-matter description to novel spectroscopies. *Nat. Rev. Chem.* **2**, 0118 (2018).
13. D. N. Basov, R. D. Averitt, D. Hsieh, Towards properties on demand in quantum materials. *Nat. Mater.* **16**, 1077–1088 (2017).
14. M. Rini, R. Tobey, N. Dean, J. Itatani, Y. Tomioka, Y. Tokura, R. W. Schoenlein, A. Cavalleri, Control of the electronic phase of a manganite by mode-selective vibrational excitation. *Nature* **449**, 72–74 (2007).
15. M. Först, C. Manzoni, S. Kaiser, Y. Tomioka, Y. Tokura, R. Merlin, A. Cavalleri, Nonlinear phononics as an ultrafast route to lattice control. *Nat. Phys.* **7**, 854–856 (2011).
16. J. Zhang, R. D. Averitt, Dynamics and control in complex transition metal oxides. *Annu. Rev. Mat. Res.* **44**, 19–43 (2014).
17. M. Mitrano, A. Cantaluppi, D. Nicoletti, S. Kaiser, A. Perucchi, S. Lupi, P. Di Pietro, D. Pontiroli, M. Riccò, S. R. Clark, D. Jaksch, A. Cavalleri, Possible light-induced superconductivity in K_3C_{60} at high temperature. *Nature* **530**, 461–464 (2016).
18. M. Knap, M. Babadi, G. Refael, I. Martin, E. Demler, Dynamical Cooper pairing in nonequilibrium electron-phonon systems. *Phys. Rev. B* **94**, 214504 (2016).
19. M. A. Sentef, A. Tokuno, A. Georges, C. Kollath, Theory of laser-controlled competing superconducting and charge orders. *Phys. Rev. Lett.* **118**, 087002 (2017).
20. E. Pomarico, M. Mitrano, H. Bromberger, M. A. Sentef, A. Al-Temimy, C. Coletti, A. Stöhr, S. Link, U. Starke, C. Cacho, R. Chapman, E. Springate, A. Cavalleri, I. Gierz, Enhanced electron-phonon coupling in graphene with periodically distorted lattice. *Phys. Rev. B* **95**, 024304 (2017).
21. D. M. Kennes, E. Y. Wilner, D. R. Reichman, A. J. Millis, Transient superconductivity from electronic squeezing of optically pumped phonons. *Nat. Phys.* **13**, 479–483 (2017).
22. M. A. Sentef, Light-enhanced electron-phonon coupling from nonlinear electron-phonon coupling. *Phys. Rev. B* **95**, 205111 (2017).
23. N. Tancogne-Dejean, M. A. Sentef, A. Rubio, Ultrafast modification of Hubbard U in a strongly correlated material: Ab initio high-harmonic generation in NiO. *Phys. Rev. Lett.* **121**, 097402 (2018).
24. D. Liu, W. Zhang, D. Mou, J. He, Y.-B. Ou, Q.-Y. Wang, Z. Li, L. Wang, L. Zhao, S. He, Y. Peng, X. Liu, C. Chen, L. Yu, G. Liu, X. Dong, J. Zhang, C. Chen, Z. Xu, J. Hu, X. Chen, X. Ma, Q. Xue, X. J. Zhou, Electronic origin of high-temperature superconductivity in single-layer FeSe superconductor. *Nat. Commun.* **3**, 931 (2012).
25. W. Qing-Yan, L. Zhi, Z. Wen-Hao, Z. Zuo-Cheng, Z. Jin-Song, L. Wei, D. Hao, O. Yun-Bo, D. Peng, C. Kai, W. Jing, S. Can-Li, H. Ke, J. Jin-Feng, J. Shuai-Hua, W. Ya-Yu, W. Li-Li, C. Xi, M. Xu-Cun, X. Qi-Kun, Interface-induced high-temperature superconductivity in single unit-cell FeSe films on $SrTiO_3$. *Chinese Phys. Lett.* **29**, 037402 (2012).
26. D. Huang, J. E. Hoffman, Monolayer FeSe on $SrTiO_3$. *Annu. Rev. Condens. Matter Phys.* **8**, 311–336 (2017).
27. J. J. Lee, F. T. Schmitt, R. G. Moore, S. Johnston, Y.-T. Cui, W. Li, M. Yi, Z. K. Liu, M. Hashimoto, Y. Zhang, D. H. Lu, T. P. Devereaux, D.-H. Lee, Z.-X. Shen, Interfacial mode coupling as the origin of the enhancement of T_c in FeSe films on $SrTiO_3$. *Nature* **515**, 245–248 (2014).
28. L. Rademaker, Y. Wang, T. Berlijn, S. Johnston, Enhanced superconductivity due to forward scattering in FeSe thin films on $SrTiO_3$ substrates. *New J. Phys.* **18**, 022001 (2016).
29. S. Zhang, J. Guan, X. Jia, B. Liu, W. Wang, F. Li, L. Wang, X. Ma, Q. Xue, J. Zhang, E. W. Plummer, X. Zhu, J. Guo, Role of $SrTiO_3$ phonon penetrating into thin FeSe films in the enhancement of superconductivity. *Phys. Rev. B* **94**, 081116(R) (2016).
30. Y. Zhou, A. J. Millis, Dipolar phonons and electronic screening in monolayer FeSe on $SrTiO_3$. *Phys. Rev. B* **96**, 054516 (2017).
31. Y. Wang, L. Rademaker, E. Dagotto, S. Johnston, Phonon linewidth due to electron-phonon interactions with strong forward scattering in FeSe thin films on oxide substrates. *Phys. Rev. B* **96**, 054515 (2017).
32. Q. Song, T. L. Yu, X. Lou, B. P. Xie, H. C. Xu, C. H. P. Wen, Q. Yao, S. Y. Zhang, X. T. Zhu, J. D. Guo, R. Peng, D. L. Feng, Phonon-enhanced superconductivity at the FeSe/$SrTiO_3$ interface; arXiv:1710.07057 (2017).
33. J. Jandke, F. Yang, P. Hlobil, T. Engelhardt, D. Rau, K. Zakeri, C. Gao, J. Schmalian, W. Wulfhekel, Unconventional pairing in single FeSe layers; arXiv:1710.08861 (2017).
34. D.-H. Lee, What makes the T_c of FeSe/$SrTiO_3$ so high? *ChinesePhys. B* **24**, 117405 (2015).
35. M. L. Kuli, O. V. Dolgov, The electron-phonon interaction with forward scattering peak is dominant in high *Tc* superconductors of FeSe films on $SrTiO_3$ (TiO_2). *New J. Phys.* **19**, 013020 (2017).
36. Y. Todorov, A. M. Andrews, R. Colombelli, S. De Liberato, C. Ciuti, P. Klang, G. Strasser, C. Sirtori, Ultrastrong light-matter coupling regime with polariton dots. *Phys. Rev. Lett.* **105**, 196402 (2010).
37. Y. Todorov, C. Sirtori, Few-electron ultrastrong light-matter coupling in a quantum LC circuit. *Phys. Rev. X* **4**, 041031 (2014).
38. J. B. Curtis, Z. M. Raines, A. A. Allocca, M. Hafezi, V. M. Galitski, Cavity quantum Eliashberg enhancement of superconductivity; arXiv:1805.01482 (2018).
39. S. De Liberato, Virtual photons in the ground state of a dissipative system. *Nat. Commun.* **8**, 1465 (2017).
40. H. Bahsoun, T. Chervy, A. Thomas, K. Börjesson, M. Hertzog, J. George, E. Devaux, C. Genet, J. A. Hutchison, T. W. Ebbesen, Electronic light-matter strong coupling in nanouidic Fabry-Pérot cavities. *ACS Photonics* **5**, 225–232 (2018).
41. G. D. Mahan, *Many-Particle Physics* (Springer, 2000).
42. W. Zhong, R. D. King-Smith, D. Vanderbilt, Giant LO-TO splittings in perovskite ferroelectrics. *Phys. Rev. Lett.* **72**, 3618–3621 (1994).
43. D. Allender, J. Bray, J. Bardeen, Model for an exciton mechanism of superconductivity. *Phys. Rev. B* **7**, 1020–1029 (1973).
44. F. P. Laussy, A. V. Kavokin, I. A. Shelykh, Exciton-polariton mediated superconductivity. *Phys. Rev. Lett.* **104**, 106402 (2010).
45. O. Cotlet, S. Zeytinoğlu, M. Sigrist, E. Demler, A. Imamoğlu, Superconductivity and other collective phenomena in a hybrid Bose-Fermi mixture formed by a polariton condensate and an electron system in two dimensions. *Phys. Rev. B* **93**, 054510 (2016).
46. A. Kumar, S. Johnston, A. F. Kemper, Identifying a forward scattering superconductor through pump-probe spectroscopy; arXiv:1712.10019 (2017).
47. M. Ruggenthaler, J. Flick, C. Pellegrini, H. Appel, I. V. Tokatly, A. Rubio, Quantum-electrodynamical density-functional theory: Bridging quantum optics and electronic-structure theory. *Phys. Rev. A* **90**, 012508 (2014).
48. F. Schlawin, A. Cavalleri, D. Jaksch, Cavity-mediated electron-photon superconductivity; arXiv:1804.07142 (2018).

Acknowledgments: Discussions with H. Appel, S. Johnston, S. Latini, A. J. Millis, and L. Rademaker are gratefully acknowledged. **Funding:** M.A.S. acknowledges financial support from the DFG through the Emmy Noether Programme (SE 2558/2-1). A.R. acknowledges financial support from the European Research Council (ERC-2015-AdG-694097), Grupos Consolidados (IT578-13), and the European Union's H2020 program under GA no. 676580 (NOMAD). **Author contributions:** M.A.S. performed the calculations. M.A.S. and M.R. developed the model, with critical feedback from A.R. The idea of cavity-enhanced electron-phonon coupling was conceived by all authors while developing the implications of cavity QED density functional theory to materials. All authors discussed the results and wrote the manuscript. **Competing interests:** The authors declare that they have no competing interests. **Data and materials availability:** All data needed to evaluate the conclusions in the paper are present in the paper and/or the Supplementary Materials. All data generated and analyzed during this study are available from the corresponding author upon reasonable request.

Submitted 6 July 2018
Accepted 30 October 2018
Published 30 November 2018
10.1126/sciadv.aau6969

Citation: M. A. Sentef, M. Ruggenthaler, A. Rubio, Cavity quantum-electrodynamical polaritonically enhanced electron-phonon coupling and its influence on superconductivity. *Sci. Adv.* **4**, eaau6969 (2018).

Cavity quantum-electrodynamical polaritonically enhanced electron-phonon coupling and its influence on superconductivity

M. A. Sentef, M. Ruggenthaler and A. Rubio

Sci Adv **4** (11), eaau6969.
DOI: 10.1126/sciadv.aau6969